Comparison of feature-based indices derived from photoplethysmogram recorded from different body locations during lower body negative pressure

Shrikant Chand[1*], Neng-Tai Chiu[2*], Yun-Hsin Chou[2], Aymen Alian[3], Kirk Shelley[3], and Hau-Tieng Wu[4]

[1] *Department of Mathematics, Duke University, Durham, NC, USA*

[2] *School of Medicine, National Yang Ming Chiao Tung University, Taiwan*

[3] *Department of Anesthesiology, Yale University, New Haven, CT, USA*

[4] *Courant Institute of Mathematical Sciences, New York University, New York, NY, USA*

[*] *These authors contribute equally to this work.*

Correspondence to:

Aymen Alian, Department of Anesthesiology, Yale School of Medicine, New Haven, Connecticut, United States of America. Email: aymen.alian@yale.edu

Hau-Tieng Wu, Department of Mathematics, Courant Institute of Mathematical Sciences, New York University, New York, New York, United States of America. Email: hauwu@cims.nyu.edu

Funding: NONE.

Conflicts of Interests/Financial Disclosures: NONE

Author's contributions: SC, NTC, YHC: data analysis and write-up. AA: idea, literature review, data collection, and write-up. KS: idea, literature review, data collection, and write-up. HTW: idea, literature review, data analysis, and write-up.

Abstract

Objective: Various time domain features, including dicrotic notch (**dic**), in photoplethysmogram (PPG), and the pulse transit time (PTT) determined using the simultaneously recorded electrocardiogram (ECG), are believed to have a critical role with many potential clinical applications. However, the dependence of these parameters on PPG sensor location is less well known.

Approach: Three pulse oximetry probes (Xhale) were put simultaneously on the ear, nose, and finger in 36 healthy volunteers recruited for the lower body negative pressure (LBNP) experiment. The end point of the experiment is either the end of the -75 mmHg phase or development of hypoperfusion symptoms, whichever came first. Various features in the time domain of the recorded PPG signals were analyzed from the ear, nasal, and finger PPG at different LBNP phases. The simultaneously recorded finger PPG and ECG (Nellcor) is utilized to evaluate the dependence of PTT on the PPG sensor location.

Results: The signal quality is different among PPG signals recorded from different sites with the nasal and ear PPGs having the highest and lowest qualities respectively. Most feature-related indices evaluated from different sites are different, except pulse rate (PR). Specifically, the ratios of detectable **dic** are different, with finger and nasal PPGs being the highest and lowest respectively, and when **dic** is detectable, the e point and **dic** are also significantly different. Pulse rate variability-related indices and PTT exhibit differences when evaluated from different body locations, while we cannot conclude the behavior of PTT during different LBNP experimental phases.

Conclusion: Indices derived from PPG signals depend on where the PPG sensor is

placed on the body. Researchers should exercise caution when extrapolating conclusions from PPG recordings taken at one body location to those obtained from a different location. This is particularly crucial in the digital health era, characterized by the proliferation of mobile devices equipped with PPG sensors positioned across various body sites.

1. Introduction

Photoplethysmography (PPG) is a non-invasive technique that measures relative blood volume changes in the blood vessels [1, 2]. In addition to its wide application in oxygen saturation evaluation, it contains rich information, like heart rate, heart rate variability, respiration [2, 3], venous oxygenation [4], sympathetic nervous system activity [5] and thermoregulation [6]. As an oscillatory signal, PPG contains a cardiac component that is attributed to hemodynamics. It has been shown that a proper quantification of features of the cardiac component could be beneficial for clinical practice from the perspective of hemodynamics. For example, the compensatory reserve index derived from the PPG can be used to detect blood loss [7] and the harmonic phase information of the cardiac component has been shown to have potential as an early predictor of acute hemorrhage [8] and as an early indicator of central hypovolemia [9]. Recently, researchers have even considered extracting blood pressure information from PPG [10].

A common approach for extracting hemodynamic information from PPG involves analyzing various features within cardiac cycles [11]. Commonly utilized features in a PPG cardiac cycle are outlined in Figure 1, where we follow the terminology used in Figure 4.13 in [12]. The timestamp corresponding to the maximum of the first derivative of the PPG signal during the upper stroke of a cardiac cycle is denoted as **msp** (maximum slope point). The peak situated between the upslope and downslope is termed the **sys**-peak (systolic peak), with the upslope representing the systolic phase, initiated by ventricular pressure transmission, and the downslope signifying the diastolic phase, associated with the slowdown of blood ejection from the ventricles. The local minimum between **sys** and the previous **sys** is called the pulse onset (**onset**). The peak in the downslope with a deflection, if exists,

is called the ***dia**-peak* (diastolic peak), and the deflection point (or notch) is called the *dicrotic notch (**dic**)*. The area under the curve is also informative. The area under the curve (and above the line interpolated between the ith and the next **onset**'s) between **onset** and **dic** (**dic** and the next **onset** respectively) is called A1 (A2 respective), which is shown as the green (pink respectively) area in Figure 1. With the above-mentioned features, researchers design various indices to study hemodynamic status. A typical example is the reflective index (RI), which is defined as the ratio of the heights of **sys** and **dia** [13, 14]. RI is a measure of pulse wave reflection and the small vessel tone, and it is a more reliable index of the effect of vasoactive drugs. Another example is the stiffness index (SI), which is defined by the ratio of the subject height and the time delay between **sys** and **dia** [15, 16]. SI is viewed as an effective marker of large artery stiffness and vascular aging, and it is strongly correlated with the central pulse wave velocity. Moreover, its relationship with the mean pulmonary artery pressures and coronary heart disease have been reported in [17, 18], among others. When electrocardiogram (ECG) is available, the pulse transit time (PTT) can be calculated as the time difference between R peak and **msp**, which is approximately inversely proportional to the blood pressure and could be used to predict blood pressure [19]. More applications can be found in, for example [20]. Features-related indices considered in this paper are summarized in Table 1.

Although the feature-based approach is common, ample evidence suggests varying behaviors in PPG signals from different body sites [8, 21-24]. This raises concerns about the compatibility of indices derived from diverse PPG signal sources, particularly with the proliferation of PPG-based mobile devices on different body locations [25]. The first natural question regards the consistency or comparability of a feature-related index across diverse body locations where PPG signals are recorded. It is important to acknowledge that certain features, such as **dia** and **dic**, may not always

be present, as discussed in arterial blood pressure literature [7]. In such cases, a common approach involves using the e point derived from the second-order differentiation of PPG as a substitute. However, as **dic** may appear in one cycle and vanish in the next (see Figure 1 for an example, where **dic** is different from the e point), the accuracy of the e point's positioning as a **dic** surrogate is crucial to avoid potential errors. The second natural question to ask is thus how different the **dic** and the e point are in different body locations. Another relevant topic is the potential existence of multiple local maxima around **sys**, complicating the determination of **sys** and consequently affecting indices reliant on it. See Figure 2 for an example. Given that **sys** and **msp** are typical features used to assess pulse rate (PR) and pulse rate variability (PRV), our third question is about the variance in PR and PRV indices evaluated using **msp** or **sys** across different body locations.

In this study, we investigate these questions through PPG signals simultaneously recorded from various body sites, such as the ear, nose, and finger, during a lower body negative pressure (LBNP) experiment through an integrated data acquisition system and consistent sensors from the same manufacturer. We assess various feature-related indices outlined in Table 1, along with the phase harmonic index (PHI) and amplitude harmonic index (AHI), which are derived from the harmonic phase and amplitude of the cardiac component in the ear PPG signal, employing time-frequency analysis for a comprehensive examination of hypovolemia created with lower body negative pressure [8].

2. Material

We use a database collected from the LBNP study carried out in Yale-New Haven hospital. All procedures performed in studies involving human participants were in accordance with the ethical standards of the institutional and/or national

research committee and with the 1964 Helsinki declaration and its later amendments or comparable ethical standards. The Human Investigation Committee of the Yale School of Medicine approved the study protocol 2000020057. The clinical trial number is NCT 03592290. There are 36 healthy subjects (19 males and 17 females) with ages 18-40 recruited for the study. Exclusion criteria included current pregnancy or any history of pulmonary, cardiac, or vascular disease, including hypertension. A negative pregnancy test was confirmed for all female subjects. Subjects were instructed to refrain from consuming alcohol and caffeinated beverages, strenuous exercise, and tobacco consumption for at least 12 hours before the study. We focused on the Xhale SpO_2 sensors (Xhale, Inc., Gainesville, FL) that were used to monitor PPG waveforms at the ear, nasal, and finger using identical sensors, and the Nellcor SpO_2 sensor at the finger along with the ECG sensor. All data was digitized at 100Hz and continuously recorded to a laptop computer using a data acquisition system (LabChart, ADInstruments, Version 7.2.2). Specifics regarding the setup of the LBNP apparatus and the study environment have been previously described in detail [26] and we refer readers with interest there.

3. Methods and statistics

We start with detailing the algorithm that automatically annotates features of interest. Assume that the PPG is sampled uniformly with the period $\Delta_t > 0$ second (the sampling rate is $1/\Delta_t$ Hz). A low pass filter at 20Hz and a high pass filter at 0.5Hz are applied after mean-centering. The resulting signal is saved as a vector f. To focus on the relevant features and indices, we only consider high-quality PPG segments selected using the signal quality index (SQI) as outlined below. The PPG signals are first split into non-overlapping 5 second segments. The PPG quality for each segment is determined by the same ratio-based algorithm used in [27]. In short,

using time-frequency analysis tools, the cardiac component of the PPG signal is decomposed into its strongest five harmonics and the remaining residue. The SQI is then set to be the ratio of the strength of these harmonic components to the total signal strength, which is a value between 0 and 1. The higher the score is, the better the PPG quality is. See Figure 3 for an example of PPG segments with different SQIs. We reject segments with a score lower than 0.9 and focus on the remaining segments, which we view as high-quality, for the following analysis. We choose 0.9 as the threshold based on our previous experience for feature analysis and visual inspection that segments with SQI greater than 0.9 usually have identifiable cardiac cycles and desired features.

sys is determined as the local maximum of each cardiac cycle in the PPG signal using the standard double kernel technique. For a given cardiac cycle, **onset** is determined as the local minimum between the previous **sys** and the current **sys**. **msp** is determined from the local maximum between **onset** and **sys** in the first derivative of PPG. It is important to mention that while any numerical differentiation method may be considered [28], to be reproducible, we consistently evaluate the second derivative by carrying out two iterations of the centered finite difference method at interior points and two iterations of the forward/backward finite difference method at boundary points so that the accuracy of numerical evaluation is of order $(\Delta_t)^2$ and Δ_t in the interior and boundary points respectively. **dia** is then determined as the local maxima between **sys** and **onset** of the next cardiac cycle, if exists. Note that **dia** may not always exist. Denote t_i^{msp}, t_i^{sys} and t_i^{dia} to be the time stamps of **msp**, **sys**, and **dia**, respectively, of the i-th cardiac cycle (see **Figure 1**).

When **dia** exists, we could determine **dic** as the local minimum between **sys** and **dia**, which is determined in the following way. Evaluate the second derivative of PPG, which we call the *acceleration PPG* (APPG). We look for APPG's first local

maximum after the detected **sys**. We label this point the e point, which again we follow the notation shown in Figure 4.13 in [12]. Once the e point is detected, we look back to the original PPG signal for the local minimum in a small interval of 1/40 seconds around the e point. If it exists, we label this the **dic** and say that this cardiac cycle has a *detectable **dic***; otherwise, we call this cardiac cycle ***dic**-free*. It is important to note that when **dic** exists, we cannot simply equate **dic** and the e point, since these points have different meanings. The e point is the locally fastest changing point of the first derivative of PPG, while **dic** is the 0 point of the first derivative of PPG, and they may sit in different locations. Suppose there are N cardiac cycles in the high-quality PPG signal and there are $M \leq N$ cycles that have detectable **dic** in the time domain, indexed as $i_1 < \cdots < i_M$, and the timestamps of these **dic**'s are denoted as $t_{i_1}^{dic} < \cdots < t_{i_M}^{dic}$. Also denote the timestamps of the e-point of all N cycles as $t_{i_1}^{e} < \cdots < t_{i_N}^{e}$ (see **Figure 1**).

With the above features, we consider the following feature-based indices. For $i = i_1, \ldots, i_N$, we take the peak-to-peak times PPT_i and $T2P_i$ as the time difference between the ith **dia** and **sys** and the ith **sys** and **msp** respectively. The reflective index (RI) is taken as the ratio between the signal height at the ith **dia** peak to the signal height at the ith **sys** peak. For $i = i_1, \ldots, i_{N-1}$, the total cycle time TT_i is taken as the time difference between the ith **msp** and the next **msp**. For $i = i_1, \ldots, i_M$, we take the **dic** to baseline time (DNB) as the time difference between the ith **dic** and the next **msp**. We also evaluate the A2 to A1 ratio, called A2A1. See Table 1 for a summary of these indices.

To evaluate PR and PRV, we consider **msp** or **sys** as the surrogate of R peak in the ECG signal. The PR is defined as the mean of the inverse of consecutive **msp**-**msp** or **sys**-**sys** intervals over 25 consecutive cardiac cycles, which we dempte as **msp**-PR or **sys**-PR. Define the interval between two consecutive **msp**'s or **sys**'s as the

pulse-to-pulse intervals (PPI), which is a surrogate of the R-peak to R-peak interval (RRI) when we study heart rate variability (HRV) in ECG signals [29]. With PPIs, we evaluate two PRV indices, the root mean square of successive differences between normal heartbeats (RMSSD) and the standard deviation of all normal R-peak to R-peak intervals (SDNN). If **msp** is used to define PPIs, we call these indices **msp**-RMSSD and **msp**-SDNN; otherwise, we call them **sys**-RMSSD and **sys**-SDNN. These indices are evaluated for non-overlapping epochs with 25 consecutive cycles over the high-quality segments.

To quantify phase and amplitude behaviors of the harmonics of a signal, we collect AHI and PHI indices which are summarized from [8]. Following the adaptive harmonic model (AHM), we suppose the PPG signal expresses a decomposition of the form

$$f(t) = \sum_{k=1}^{\infty} A_k(t) \cos(2\pi\, \phi_k(t)),$$

where $A_k(t)$ and $\phi_k(t)$ are the time-varying amplitude and phase, respectively, of the k-th harmonic component at time t. To quantify the phase behavior over a time interval I, we define the k-th phase hemodynamic index (PHI) as

$$\nabla\phi_k := median_{t\in I}(k\phi_1(t) - \phi_k(t)),$$

which is the phase discrepancy between the k-th harmonic and the fundamental component, where $k = 2,3$. Similarly, we define the k-th amplitude hemodynamic index (AHI) as

$$\nabla A_k := \frac{median_{t\in I}(A_k(t)),}{median_{t\in I}(A_1(t)),}$$

which is the phase discrepancy between the k-th harmonic and the fundamental component, where $k = 2,3$.

Finally, we examine how PTT varies with PPG sensor location. Since PTT is on the 100ms scale, to enhance the accuracy, the PPG and ECG signals are upsampled to

500Hz. Given that ECG and PPG signals were collected from different instruments, we first aligned them using the following approach. We construct the instantaneous pulse rate (IPR) from the **msp** of the PPG**,** denoted as **msp**-IPR, by applying cubic spline interpolation to the nonuniformly sampled data points $\left\{\left(t_i^{msp}, \frac{1}{t_i^{msp}-t_{i-1}^{msp}}\right)\right\}_{i=2}^{N}$, where N represents the number of cardiac cycles. Signal alignment between Nellcor and Xhale is achieved by maximizing the correlation between the **msp**-IPR derived from the Nellcor finger PPG and that from the Xhale finger PPG by shifting. Since PTT is on the scale of 100ms, to further minimize the impact of poor signal quality on PTT, beyond the applied SQI, we visually inspect the PPG signals to eliminate misclassified high-quality segments. ECG signal quality is also visually assessed, and R-peaks corresponding to RRI shorter than 0.4 s or longer than 1.5 s are excluded. Only time intervals with both high-quality PPG and ECG signals are retained for further PTT analysis. Following these preprocessing steps, the PTT of the jth cardiac cycle is calculated as the time difference between the R peak in the ECG signal and the **msp** of the associated PPG cycle. Since PTT tends to decrease with shorter RRIs and the baseline HR depends on subjects, we normalize the PTT to ensure comparability across individuals by their baseline RRI, that is, $\widehat{PTT}_j = \frac{PTT_j}{RRI_{baseline}}$, where $RRI_{baseline}$ is the median RRI during the baseline stage of the LBNP experiment.

For each of the above indices derived from each channel, including the SQI, we report the median and median absolute deviation (MAD) as it is more robust to outliers than the mean and standard deviation. For the demographic data, we report the mean and standard deviation (STD). We apply the one-way analysis of variance (ANOVA) to test the hypothesis that the means of an index derived from different body locations are equal against the alternative hypothesis that at least one body

location gives a different result from the others. To compare two methods to define an index, we apply the Wilcoxon signed-rank test. We view a p-value less than 0.005 as statistically significant [30], and use the Bonferroni correction to handle the multiple test comparison. Since we compare 15 indices in total with ANOVA, the corrected p-value is $0.005/15=3.3\times10^{-4}$.

4. Results

The dataset consists of 36 subjects (17 males and 19 females) subjects ages 18-40 underwent progressive LBNP protocol. Case #3 is missing. The overall signal length is 29.86±7m. Two flawed cases (one female "case #10" and one male "case #13") were removed due to at least one broken channel. Thus, 33 cases were included in the analysis. The first 4.5 m of case 25, 29.3-34.5 m of case #28, and the first 3.8 m of case #32 are removed due to broken signals.

In the PTT analysis, we accounted for the quality of both Xhale and Necllor devices. Besides case #10 and case#13, cases #1, #5, #6, #7, #8, #18, #19, #25, and #27 were further excluded since we fail to align Nellcor and Xhale using **msp**-IPR and case #30 was excluded as the LBNP experiment was terminated early. In total, 23 cases are included in PTT analysis.

The SQI of PPG recorded from different body locations is 0.99±0.10 (0.98±0.13 and 0.98±0.11) for nasal (ear and finger respectively). The median and MAD of SQI for each case are reported in Table 2. The null hypothesis that the signal quality scores are the same for different body locations is rejected by the one-way ANOVA test ($p<10^{-10}$). With 0.9 as the SQI threshold, 84.68% (77.68% and 80.90%) of the 5 second segments of the nasal (ear and finger respectively) PPG are considered of high quality. The percentages of cases and sensor types with an SQI above this threshold are reported in Table 2. The progression of SQI over various LBNP experimental

phases over different body locations is reported in Figure 4 with the p-value comparison reported in Table 3. It suggests that overall SQI becomes more similar across different body locations as the experiment progresses but becomes more different in the baseline and in the recovery phases. All results described below assume only signal segments with an SQI of at least 0.9 are considered.

Next, we explored **dic**. The cardiac cycles with detectable **dic** are overall 43.00±22.40% (42.50±18.57% and 66.26±16.52%) of all cardiac cycles in the nasal (ear and finger respectively) PPG. The ratios of cardiac cycles with detectable **dic** are different over different body locations with statistical significance by the one-way ANOVA test ($p < 10^{-10}$). In terms of number of cardiac cycles, there are 27,878 (21,889 and 40,549 respectively) in the nasal (ear and finger respectively) PPG that have detectable **dic** and 38,743 (39,072 and 23,166 respectively) that are **dic**-free.

We then noted the relationship between the **dic** and e point over cardiac cycles with detectable **dic** from different body locations, which is plotted In Figure 5. For those cardiac cycles with detectable **dic**, the root mean square of the time between the **dic** and e point is 17ms (14ms and 18ms respectively). In 72.93% (37.58% and 59.06% respectively) of the cardiac cycles with **dic**, the e point is strictly before the **dic** in the nasal (ear and finger respectively) PPG with the median time difference 20±8ms (10±9ms and 20±9ms respectively). In 24.70% (39.45% and 27.41% respectively) of these cycles, the e point is exactly at the **dic** in the nasal (ear and finger respectively) PPG, and in the remaining 2.38% (22.98% and 13.53% respectively), the e point is strictly after the **dic** in the nasal (ear and finger respectively) PPG with the median time difference 10±2ms (10±2ms and 10±3ms respectively). The time discrepancy among different channels is significantly different among different body locations when tested by the one-way ANOVA ($p < 10^{-10}$).

We then explored the relationship between **dic** and other features. For those

cardiac cycles with detectable **dic**, the time difference between **msp** and **dic** is 0.22±0.04s (0.22±0.05s and 0.26±0.04s respectively) in the nasal (ear and finger respectively) PPG. These time differences were different over different body locations with statistical significance by the one-way ANOVA test ($p < 10^{-10}$). The time difference between **msp** and e point over all cycles is 0.21±0.03s (0.22±0.05s and 0.25±0.04s respectively) in the nasal (ear and finger respectively) PPG. The time difference between **msp** and e in all cardiac cycles are different over different body locations with statistical significance by the one-way ANOVA test ($p < 10^{-10}$).

Continuing, we explored feature-related indices. The summary statistics of these indices derived from different body locations are shown in Table 4. In short, all indices are significantly different when evaluated from PPG signals recorded from different body locations.

Next, we report the exploration of PRV related indices. We collect segments of 25 consecutive cardiac cycles. The **msp**-PR is 1.41±0.21 bps (1.41±0.21 bps and 1.41±0.19 bps respectively) and the **sys**-PR is 1.41±0.21 bps (1.41±0.21 bps and 1.41±0.19 bps respectively) from the nasal (ear and finger respectively) PPG. For both **msp**-PR and **sys**-PR, there is no statistically significant difference among body locations when tested using the one-way ANOVA, as shown in Table 4. Using the Wilcoxon signed rank test comparing PR defined by **msp** and **sys** concludes that **msp**-PR and **sys**-PR were not significantly different in all body locations ($p = 0.99$, $p = 0.87$, and $p = 0.99$ in nasal, ear, and finger respectively). The **msp**-SDNN was 28.9±12.6ms (30.1±14.5ms and 29.6±11.9ms respectively) and the **sys**-SDNN was 29.0±12.4ms (34.4±16.9ms and 29.6±11.8ms respectively) for the nasal (ear and finger respectively) PPG. Using the Wilcoxon signed rank test comparing SDNN defined by **msp** and **sys** concludes that **msp**-SDNN and **sys**-SDNN were not significantly different for nasal and finger PPGs ($p = 0.91$ and $p = 0.96$ respectively),

but significantly different in ear PPG ($p < 10^{-10}$). The **msp**-RMSSD was 21.6±10.1ms (24.0±14.9ms and 22.8±9.2ms respectively) and the **sys**-RMSSD was 24.9±13.1ms (34.5±23.5ms and 23.4±9.9ms respectively) for the nasal (ear and finger respectively) PPG. Using the Wilcoxon signed rank test comparing RMSSD defined by **msp** and **sys** concludes that **msp**-RMSSD and **sys**-RMSSD were not significantly different for finger PPG ($p = 0.11$) but significantly different for nasal and ear PPGs ($p < 10^{-10}$ for both channels). Summary statistics for PR are reported in Table 4 and PRV related indices are reported in Table 5.

We then evaluate harmonic related indices (PHI and AHI) and their statistics. See Table 6 for a summary. It shows that PHI and AHI evaluated from PPGs recorded from different body sites have significant difference [8, 21-24], which is consistent with the previous findings showing different oscillatory morphologies among PPGs recorded from different body locations.

Finally, we present the PTT analysis. The normalized PTT, calculated using Nellcor finger PPG, Xhale finger PPG, Xhale ear PPG, and Xhale nose PPG, is 0.30±0.02, 0.30±0.03, 0.23±0.03, and 0.21±0.03 (no unit), respectively. First, we show the PTT derived from Nellcor finger PPG and ECG across different LBNP stages for all subjects in the first panel of Figure 7. We cannot see a clear relationship between normalized PTT and LBNP phases. Second, we explore the PTT derived from different body locations in the second to fourth panels in Figure 7. We find statistically significant difference between the results using Nellcor finger PPG and Xhale finger PPG ($p<10^{-10}$), while the absolute error between these two PTTs is 4ms±2ms. The normalized PTT derived from Xhale finger, ear and nose PPGs are statistically different when tested with the one-way ANOVA ($p<10^{-10}$). Figure 8 shows the unnormalized PTT determined from Nellcor finger, Xhale finger, Xhale ear, and Xhale nose PPGs, which are statistically different when tested with the one-way

ANOVA ($p<10^{-10}$).

5. Discussion and conclusion

In this paper, we study a fundamental question of whether features of PPG signals recorded from different body locations are equivalent? We have several findings. The signal quality is different among PPG signals recorded from different sites. Overall, the nasal PPG has the highest quality, and ear PPG has the lowest quality. We find that even when PPGs are collected when the subjects are resting under the well-controlled experiment environment, about 9% (and 11% and 16%) of PPG segments are of low quality (SQI<0.9) for nasal, ear, and finger sensors respectively. PPGs recorded from all body locations have different ratios of detectable dicrotic notch (**dic**), with finger PPG being the highest and nasal PPG as the lowest. When **dic** is detectable, the e point and **dic** are also significantly different between different locations. Most feature-related indices and PHI and AHI are different among body locations with statistical significance, except total cycle time (TT), which is inversely related to pulse rate (PR). The other index that is not statistically different among body locations is PR. On the other hand, pulse rate variability (PRV)-related indices exhibit differences. We conclude that indices derived from PPG depend on where the PPG sensor is placed in the body. Researchers should be careful when applying conclusions established from PPG recorded from one body location to another PPG recorded from a different body location.

Since **dic** has a critical role in many applications, for example, in **dic** to baseline time (DNB), reflective index (RI) [13, 14] and stiffness index (SI) [15, 16], it is worth further discussion. There have been several algorithms proposed to automatically identify **dic**. To our knowledge, one of the earliest relevant algorithms aiming to detect **dic** in the brachial arterial pressure waveform was proposed in 1968 [31].

Several algorithms followed, including a compression scheme [32], a successive chord approach [33], the second derivatives of the waveform approach [34, 35], a rule-based logic approach [11], a nonconvex optimization approach [36, 37], a model based approach [20], etc. In general, there is no guarantee that a well-defined **dic** exists in a cardiac cycle, and when such a notch is not detectable, a dilemma appears. That is, since **dic** is *originally* defined in the time-domain by the notch by a specific morphological description, if such notch does not exist, what is **dic**? This often depends on the researcher's discretion. A traditional approach when the **dic** is undetectable is using the e point determined from the APPG as a surrogate of **dic**. However, the exploration in this paper suggests that using the e point might not be the optimal surrogate when **dic** does not exist. At first glance, the roughly 10 millisecond difference between the e point and **dic** when **dic** exists might be harmless in clinical applications, and it is always possible to replace **dic** by the e point systematically to avoid this discrepancy. However, it does not resolve the "what is **dic**" problem. A recent effort using a decomposition scheme [38] to determine the **dic** might alleviate this issue. From mathematical perspective, this decomposition could be modeled by the adaptive non-harmonic model framework [8] so that the fundamental component is suppressed and the **dic** is enhanced. While this is potential in resolving the issue of replacing **dic** by the e point, the dependence of **dic** on PPG sensor locations, and the understanding of its mechanism, still exists. We need more work to handle this challenging problem, and we will discuss it to our future work.

The study results coincide with the well-known fact that PPG recorded from different body locations capture different physiological dynamics, which is represented in the PPG morphology [8, 9, 21, 24]. For example, there are significantly more cardiac cycles (and higher ratio) in the finger PPG that have detectable **dic** compared with the ear and nasal PPGs. The time difference between **msp** and **dic** for

those cardiac cycles with detectable **dic** is significantly different in these three PPG signals. Moreover, we shall mention that PHI and AHI are evaluated using the time-frequency analysis of PPG, which encodes PPG dynamics jointly from the time and frequency domains. These findings, combined with existing literature, further confirm that PPG recorded from different body locations are different and should not be viewed as the same signal. We hypothesize that by integrating PPGs recorded from different body locations, we may obtain a more systematic understanding of the hemodynamics. We will explore this possibility in our future study.

Since PRs evaluated from PPGs recorded from different body locations are not statistically different, the discrepancy of PRV with statistical significance may initially seem concerning. We shall mention that if we view a sequence of pulse-to-pulse intervals (PPI) as a random process, the PR is its mean, and SDNN is its standard deviation. These two quantities are of different nature, so a similar PR does not imply a similar SDNN. RMSSD is the root mean square of successive PPI difference, which has a different nature compared with PPI since the finite difference operator is applied. Moreover, it is important to notice that the difference operator could amplify the discrepancy among PPIs evaluated from different PPGs. See Figure 6 for an example, where PPIs from finger-PPG and ear-PPG and their differences, denoted as dPPI, are shown. The mean and STD of the difference of these two PPIs are $<10^{-4}$ ms and 1.177 ms, and the mean and STD of the difference of these two dPPIs are -0.004 ms and 2.078 ms. As a result, it is not surprising that PRV-related indices are significantly different when evaluated from different PPIs. Given that PRV-related indices serve as crucial alternatives to HRV indices when electrocardiogram data is unavailable [39], researchers should be careful when interpreting these indices. This caution is particularly important when extrapolating results obtained from PRV-related indices evaluated from one body's location to those

evaluated from a different body location.

The findings related to PTT require further discussion. In this study, PTT measured at the ear and nose are significantly shorter than that measured at the finger, likely due to anatomical differences; that is, the arterial path to the finger is longer than to the ear or nose. Notably, we observe a statistically significant difference between PTT measured using the Nellcor finger PPG and that from the Xhale finger PPG, despite synchronizing the devices via IPR alignment. This highlights a key limitation of our PTT analysis: ECG and PPG signals were recorded using separate devices without a shared hardware clock for synchronization. Although IPR was used for temporal alignment, discrepancies between hardware systems may still introduce measurement errors. Furthermore, normalized PTT exhibited limited sensitivity to LBNP phases, even when using ECG and PPG signals both acquired from the Nellcor device. This result contrasts with previously published findings. Therefore, while we can confirm that PTT varies with measurement site, we are unable to draw stronger conclusions. It is also important to note that the Nellcor system operates as a black box [40], and we cannot rule out the possibility that its ECG and PPG signals are not synchronized sufficiently for accurate PTT analysis, as has been reported for other commercial systems [41].

There are more limitations in this work. First, all PPGs are recorded when the subjects are resting during a standardized LBNP experiment. A natural question to ask is if the same conclusion holds for signals recorded when a subject is moving or even running, which are nowadays scenarios that are getting more and more common. In the free-living environment, the SQI will also be worse, which increases the signal analysis challenge. Second, we only explore part of the available indices researchers use in practice, and the conclusion may not be extrapolated to the unexplored indices. For example, while the PR and two PRV-related indices we explore here seem to be

independent of body locations, other PRV-related indices might have dependence, particularly those that depend on higher order derivatives. Third, the population is limited to young subjects. Are the same conclusions carried over to older subjects? Moreover, while it is intuitively correct that features depend on body locations, the physiological mechanisms are not yet well known. Exploring these interesting topics will be reported in our future work.

Reference

1. Allen, J., *Photoplethysmography and its application in clinical physiological measurement.* Physiol Meas, 2007. **28**(3): p. R1-39.
2. Alian, A.A. and K.H. Shelley, *Photoplethysmography.* Best Pract Res Clin Anaesthesiol, 2014. **28**(4): p. 395-406.
3. Starmer, C.F., P.A. McHale, and J.C. Greenfield, Jr., *Processing of arterial pressure waves with a digital computer.* Comput Biomed Res, 1973. **6**(1): p. 90-6.
4. Walton, Z.D., et al., *Measuring venous oxygenation using the photoplethysmograph waveform.* Journal of clinical monitoring and computing, 2010. **24**(4): p. 295-303.
5. Budidha, K. and P.A. Kyriacou, *Photoplethysmography for Quantitative Assessment of Sympathetic Nerve Activity (SNA) During Cold Stress.* Frontiers in Physiology, 2019. **9**.
6. Larsen, P.D., et al., *Spectral analysis of AC and DC components of the pulse photoplethysmograph at rest and during induction of anaesthesia.* Int J Clin Monit Comput, 1997. **14**(2): p. 89-95.
7. Convertino, V.A., et al., *Individual-Specific, Beat-to-beat Trending of Significant Human Blood Loss: The Compensatory Reserve.* Shock, 2015. **44 Suppl 1**: p. 27-32.
8. Alian, A., K. Shelley, and H.T. Wu, *Amplitude and phase measurements from harmonic analysis may lead to new physiologic insights: lower body negative pressure photoplethysmographic waveforms as an example.* J Clin Monit Comput, 2023. **37**(1): p. 127-137.
9. Eid, A.M., et al., *Using the ear photoplethysmographic waveform as an early indicator of central hypovolemia in healthy volunteers utilizing LBNP induced hypovolemia model.* Physiol Meas, 2023. **44**(5).
10. Salah, M., et al., *Beat-Based PPG-ABP Cleaning Technique for Blood Pressure Estimation.* IEEE Access, 2022. **10**: p. 55616-55626.
11. Oppenheim, M.J. and D.F. Sittig, *An innovative dicrotic notch detection algorithm which combines rule-based logic with digital signal processing techniques.* Computers and biomedical research, 1995. **28**(2): p. 154-170.
12. Kyriacou, P.A. and J. Allen, *Photoplethysmography: Technology, Signal Analysis and Applications*. 2021: Elsevier Science.
13. Millasseau, S.C., et al., *Determination of age-related increases in large artery stiffness by digital pulse contour analysis.* Clinical science, 2002. **103**(4): p. 371-377.
14. Millasseau, S.C., et al., *The vascular impact of aging andvasoactive drugs:*

Comparison of two digital volume pulse measurements. American journal of hypertension, 2003. **16**(6): p. 467-472.

15. Woodman, R., et al., *Interpretation of the digital volume pulse: its relationship with large and small artery compliance.* Clinical Science, 2003. **104**(3): p. 283-284.
16. Gunarathne, A., et al., *Measurement of stiffness index by digital volume pulse analysis technique: clinical utility in cardiovascular disease risk stratification.* American journal of hypertension, 2008. **21**(8): p. 866-872.
17. Chemla, D., et al., *Matching dicrotic notch and mean pulmonary artery pressures: implications for effective arterial elastance.* American Journal of Physiology-Heart and Circulatory Physiology, 1996. **271**(4): p. H1287-H1295.
18. Dawber, T.R., H.E. THomas Jr, and P.M. McNamara, *Characteristics of the dicrotic notch of the arterial pulse wave in coronary heart disease.* Angiology, 1973. **24**(4): p. 244-255.
19. Gao, M., N.B. Olivier, and R. Mukkamala, *Comparison of noninvasive pulse transit time estimates as markers of blood pressure using invasive pulse transit time measurements as a reference.* Physiological reports, 2016. **4**(10): p. e12768.
20. Hoeksel, S., et al., *Detection of dicrotic notch in arterial pressure signals.* Journal of clinical monitoring, 1997. **13**(5): p. 309-316.
21. Awad, A.A., et al., *Different responses of ear and finger pulse oximeter wave form to cold pressor test.* Anesth Analg, 2001. **92**(6): p. 1483-6.
22. Eid, A.-M., et al., *Using the ear photoplethysmographic waveform as an early indicator of central hypovolemia in healthy volunteers utilizing LBNP induced hypovolemia model.* Physiological Measurement, 2023. **44**(5): p. 055008.
23. Shelley, K.H., et al., *The effect of venous pulsation on the forehead pulse oximeter wave form as a possible source of error in Spo2 calculation.* Anesth Analg, 2005. **100**(3): p. 743-747.
24. Awad, A.A., et al., *Analysis of the ear pulse oximeter waveform.* J Clin Monit Comput, 2006. **20**(3): p. 175-84.
25. Castaneda, D., et al., *A review on wearable photoplethysmography sensors and their potential future applications in health care.* Int J Biosens Bioelectron, 2018. **4**(4): p. 195-202.
26. Alian, A.A., et al., *Impact of central hypovolemia on photoplethysmographic waveform parameters in healthy volunteers. Part 1: time domain analysis.* J Clin Monit Comput, 2011. **25**(6): p. 377-85.
27. Chiu, N.-T., et al., *Signal quality assessment of peripheral venous pressure.* Journal of clinical monitoring and computing, 2023.

28. Zwillinger, D., *CRC Standard Mathematical Tables and Formulae*. 2002: CRC Press.
29. *Heart rate variability: standards of measurement, physiological interpretation and clinical use. Task Force of the European Society of Cardiology and the North American Society of Pacing and Electrophysiology.* Circulation, 1996. **93**(5): p. 1043-65.
30. Benjamin, D.J., et al., *Redefine statistical significance.* Nature Human Behaviour, 2018. **2**(1): p. 6-10.
31. Kyle, M.C., J.D. Klingeman, and E.D. Freis, *Computer identification of branchial arterial pulse waves.* Comput Biomed Res, 1968. **2**(2): p. 151-9.
32. Glaeser, D., et al., *A hierarchical minicomputer system for continuous post-surgical monitoring.* Computers and Biomedical Research, 1975. **8**(4): p. 336-361.
33. Kinias, P., H. Fozzard, and M. Norusis, *A real-time pressure algorithm.* Computers in biology and medicine, 1981. **11**(4): p. 211-220.
34. Chakraborty, A., D. Sadhukhan, and M. Mitra, *Accurate detection of dicrotic notch from PPG signal for telemonitoring applications.* Int J Biomed Eng Technol, 2018.
35. Starmer, C.F., P.A. McHale, and J.C. Greenfield Jr, *Processing of arterial pressure waves with a digital computer.* Computers and Biomedical Research, 1973. **6**(1): p. 90-96.
36. Fleischhauer, V., et al., *Pulse decomposition analysis in photoplethysmography imaging.* Physiological Measurement, 2020. **41**(9): p. 095009.
37. Huang, S.-C., et al. *Decomposition analysis of digital volume pulse signal using multi-model fitting*. in *XIII Mediterranean Conference on Medical and Biological Engineering and Computing 2013*. 2014. Springer.
38. Pal, R., et al., *An algorithm to detect dicrotic notch in arterial blood pressure and photoplethysmography waveforms using the iterative envelope mean method.* medRxiv, 2024: p. 2024.03.05.24303735.
39. Lu, S., et al., *Can Photoplethysmography Variability Serve as an Alternative Approach to Obtain Heart Rate Variability Information?* Journal of Clinical Monitoring and Computing, 2008. **22**(1): p. 23-29.
40. Ruskin, K.J. and K.H. Shelley, *Patent medicine and the "black box"*. 2005, LWW. p. 1361-1362.
41. Lin, Y.-T., et al., *Unexpected sawtooth artifact in beat-to-beat pulse transit time measured from patient monitor data.* PloS one, 2019. **14**(9): p. e0221319.

Table 1: Feature related indices and their definitions, where f is the PPG signal.

Feature-related Index	Description
$PPT_i = t_i^{dia} - t_i^{sys}$	**sys** to **dia** time.
$T2P_i = t_i^{sys} - t_i^{msp}$	**msp** to **sys** time.
$RI_i = \frac{f(t_i^{dia})}{f(t_i^{sys})}$	**dia** to **sys** height ratio.
$TT_i = t_{i+1}^{msp} - t_i^{msp}$	Total cycle time. Only values less than 1.5 will be analyzed to avoid outliers.
$DNB_{i_m} = t_{i_m+1}^{msp} - t_{i_m}^{dic}$	**dic** to baseline time. It is only evaluated when there is a detectable **dic**. Only values less than 1 will be analyzed to avoid outliers.
$A2A1_i = \frac{\int_{t_{i_m}^{dic}}^{t_{i_m+1}^{msp}} (f(s) - g(s))ds}{\int_{t_{i_m}^{msp}}^{t_{i_m}^{dic}} (f(s) - g(s))ds}$, where $g(s) = \frac{f\left(t_{i_m+1}^{msp}\right) - f\left(t_{i_m}^{msp}\right)}{t_{i_m+1}^{msp} - t_{i_m}^{msp}} \times \left(s - t_{i_m}^{msp}\right) + f(t_{i_m}^{msp})$	Area 2 to Area 1 ratio, where Area 1 and Area 2 are areas between signal and interpolated line between two consecutive onset. It is only evaluated when there is a detectable DN. Only those cycles with $\boldsymbol{t_{i_m+1}^{msp} - t_{i_m}^{msp} < 1.5}$ will be analyzed to avoid outliers.
$RMSSD_j = \sqrt{\frac{1}{24}\sum_{i=j}^{24}\left(PPI_i^{R_h} - PPI_{i-1}^{R_h}\right)^2}$	Root mean square of successive pulse to pulse interval differences (h=0 means we use **msp** and h=1 means we use **sys**). The RMSSD is taken over cycles of 25 consecutive peaks. The unit is milliseconds.
$SDNN_j = \sqrt{\frac{1}{25}\sum_{i=j}^{25}\left(PPI_i^{R_h} - \overline{PPI^{R_h}}\right)^2}$	Standard deviation of successive pulse to pulse interval (h=0 means we use **ms** and h=1 means we use **sys**) over cycles of 25 consecutive peaks, where $\overline{PPI^{R_h}}$ is

	the mean. The unit is minisecond.
$PTT_j = t_j^{msp} - t_j^R$	The time difference between the R peak (t_j^R) in the simultaneously recorded ECG signal and **msp** of the associated cardiac cycle in the PPG signal.

Table 2: Summary statistics of SQI for each subject. The second to fifth columns are the median±MAD of SQI, and the sixth to eighth columns are the percentage of high SQI (>0.9).

Case	**Nasal (a.u)**	**Ear (a.u)**	**Finger (a.u)**	**Nasal (%)**	**Ear (%)**	**Finger (%)**
1	0.99±0.09	0.99±0.05	0.99±0.06	88.25	87.75	87.00
2	0.98±0.06	0.93±0.12	0.97±0.04	88.63	61.50	89.41
4	0.99±0.09	0.98±0.08	0.99±0.07	80.93	84.47	73.02
5	0.98±0.09	0.96±0.09	0.97±0.10	74.87	69.54	70.30
6	0.99±0.01	0.99±0.03	0.99±0.02	98.95	95.03	96.60
7	0.99±0.05	0.99±0.06	0.76±0.09	88.94	87.19	3.02
8	0.98±0.08	0.91±0.16	0.99±0.02	82.44	53.32	97.64
9	0.98±0.03	0.98±0.08	0.98±0.05	91.88	80.11	88.80
11	0.99±0.11	0.99±0.10	0.99±0.02	78.72	79.01	95.63
12	0.99±0.03	0.99±0.02	0.99±0.02	93.88	95.72	97.55
14	0.99±0.02	0.99±0.05	0.99±0.01	96.86	90.00	99.43
15	0.95±0.03	0.92±0.12	0.92±0.07	84.51	57.04	60.92
16	0.99±0.04	0.80±0.21	0.98±0.03	94.70	16.51	94.08
17	1.00±0.04	1.00±0.03	0.80±0.18	92.18	95.24	34.69
18	0.97±0.09	0.97±0.09	0.87±0.13	78.06	79.31	38.24
19	0.99±0.03	0.98±0.07	0.69±0.18	95.74	82.98	20.57
20	0.99±0.04	0.98±0.06	0.98±0.02	94.79	82.99	95.14
21	0.99±0.03	0.93±0.16	0.99±0.05	94.99	57.23	89.09
22	0.99±0.01	0.96±0.13	0.98±0.06	98.41	71.75	85.71
23	0.99±0.09	0.98±0.04	0.98±0.10	79.63	91.90	72.69
24	0.99±0.02	0.97±0.07	0.99±0.01	97.16	80.85	99.29
25	0.99±0.03	0.86±0.14	0.99±0.16	96.31	28.11	100.00

26	0.99±0.04	0.97±0.12	0.99±0.01	94.08	74.67	99.67
27	0.93±0.13	0.95±0.10	0.79±0.15	54.95	60.75	28.33
28	0.34±0.31	0.99±0.08	0.98±0.07	21.04	96.30	92.89
29	0.99±0.09	0.99±0.05	0.99±0.06	88.28	87.53	87.03
30	0.99±0.07	0.73±0.13	0.98±0.04	88.61	0.00	95.02
31	0.99±0.03	1.00±0.01	0.99±0.04	91.27	99.44	92.39
32	0.99±0.02	0.99±0.05	0.99±0.11	96.34	93.29	99.09
33	1.00±0.02	1.00±0.03	0.99±0.01	97.02	96.03	98.34
34	0.98±0.06	0.99±0.05	0.98±0.04	88.55	89.16	94.58
35	0.99±0.04	1.00±0.01	0.99±0.04	92.44	98.04	91.60
36	0.98±0.07	0.98±0.07	0.99±0.08	84.08	87.15	85.47
All	0.99±0.10	0.98±0.13	0.98±0.11	84.68	77.68	80.90

Table 3: p-values (ANOVA) and q-values (Tukey's Honestly Significant Difference Test) for SQI comparison over different experimental phases. * and # indicate we reject the null hypothesis that group means are the same with statistical significance ($p < 0.05/3$ using the Bonferroni correction and $q < 0.05$). Multiple comparison values are calculated under Tukey's Honestly Significant Difference test.

		Multiple Comparisons		
Experimental Stages	**ANOVA-1**	**Ear vs. Finger**	**Ear vs. Nasal**	**Finger vs. Nasal**
Baseline	6.22e-6 *	6.29e-3 #	0.172	3.66e-6 #
LRT	1.05e-2 *	8.75e-2	9.5e-3 #	0.692
-15	6.50e-5 *	8.77e-2	3.20e-5 #	5.71e-2
-30	1.00e-2 *	0.100	0.630	8.48e-3 #
-45	8.72e-2	0.752	0.315	7.64e-2
-60	3.60e-3 *	3.65e-3 #	0.708	4.01e-2 #
Recovery	< 1e-10 *	2.55e-3 #	3.80e-9 #	< 1e-10 #

Table 4: Summary statistics of the considered feature-related indices. All values are Median ± MAD and are taken for cycles with an SQI above or equal to 0.9. * indicates rejecting the null hypothesis that means are equal (p<0.005/14=3.6e-4).

Value	Nasal	Ear	Finger	p value
PPT (s)	0.16±0.05	0.13±0.07	0.23±0.05	$< 10^{-10}$ *
T2P (s)	0.12±0.04	0.19±0.05	0.11±0.02	$< 10^{-10}$ *
RI (n.u.)	0.42±0.37	0.57±1.33	0.13±0.26	4.5×10^{-6} *
TT (s)	0.73±0.12	0.73±0.12	0.72±0.12	9.8×10^{-4}
DNB (s)	0.49±0.14	0.5±0.14	0.45±0.16	$< 10^{-10}$ *
A2A1 (n.u.)	0.67±0.18	0.96±0.42	0.44±0.17	$< 10^{-10}$ *
msp-PR (ms)	1.41±0.21	1.41±0.21	1.41±0.19	0.25
sys-PR (ms)	1.41±0.21	1.41±0.21	1.41±0.19	0.24

Table 5: Pulse rate variabilities evaluated using different features (**msp** and **sys**) derived from different body locations (nasal, ear and finger). All values are shown in Median ± MAD and are taken for cycles with an SQI above or equal to 0.9. The Wilcoxon rank test is used to compare the use of **msp** vs **sys** as indices under the null hypothesis of equal medians, where # indicates rejecting the null hypothesis that means are equal (p<0.005/6=8.3e-4). * indicates rejecting the null hypothesis that means are equal (p<0.005/4=1.3e-3). The unit of both SDNN and RMSSD is milliseconds (ms).

	Nasal	**Ear**	**Finger**	**p value**
msp-SDNN (ms)	28.92±12.58	30.07±14.49	29.62±11.88	9.7×10^{-4} *
sys-SDNN (ms)	29.04±12.36	34.39±16.87	29.62±11.77	$< 10^{-10}$ *
p value	0.91	$< 10^{-10}$ #	0.96	
	Nasal	**Ear**	**Finger**	**p value**
msp-RMSSD (ms)	21.57±10.08	23.96±14.91	22.84±9.19	$< 10^{-10}$ *
sys-RMSSD (ms)	24.93±13.11	34.52±23.48	23.41±9.86	$< 10^{-10}$ *
p value	$< 10^{-10}$ #	$< 10^{-10}$ #	0.11	

Table 6: AHI and PHI evaluated derived from different body locations (nasal, ear and finger). All values are shown in Median ± MAD and are taken for cycles with an SQI above or equal to 0.9. * indicate rejecting the null hypothesis that medians are equal ($p<0.05/14=3.6e-4$).

	Nasal	**Ear**	**Finger**	**p value**
PHI2 (radian)	1.77±0.72	2.16±0.95	1.36±0.71	$< 10^{-10}$ *
PHI3 (radian)	1.80±2.95	-2.07±1.65	2.22±1.43	$< 10^{-10}$ *
AHI2 (a.u)	0.50±0.21	0.38±0.2	0.59±0.2	$< 10^{-10}$ *
AHI3 (a.u)	0.26±0.08	0.19±0.08	0.25±0.09	$< 10^{-10}$ *

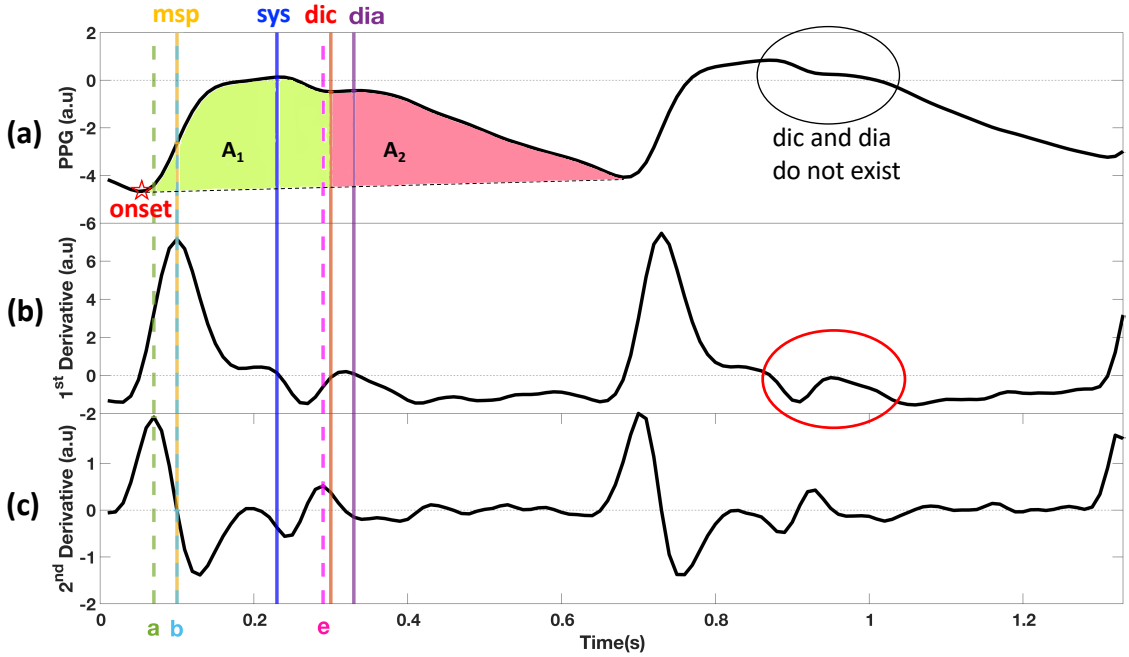

Figure 1: (a) an ear PPG signal with **onset**, **msp**, **sys**, **dic**, and **dia** marked by the intersection of the signal (in black) with the red star, yellow, dark blue, orange, and purple solid vertical lines, respectively. **(b)** The first derivative of ear PPG signal in (a), **(c)** the second derivative, sometimes called APPG, of ear PPG signal in (a) with a, b, and e points marked by the intersection of the signal with the green, light blue, and pink dashed vertical lines respectively. In this example, the second cardiac cycle does not have **dia** and **dic**, which can be observed that its first derivative is constantly negative around the region, marked by the red circle, that **dia** and **dic** should appear. a.u. means arbitrary unit.

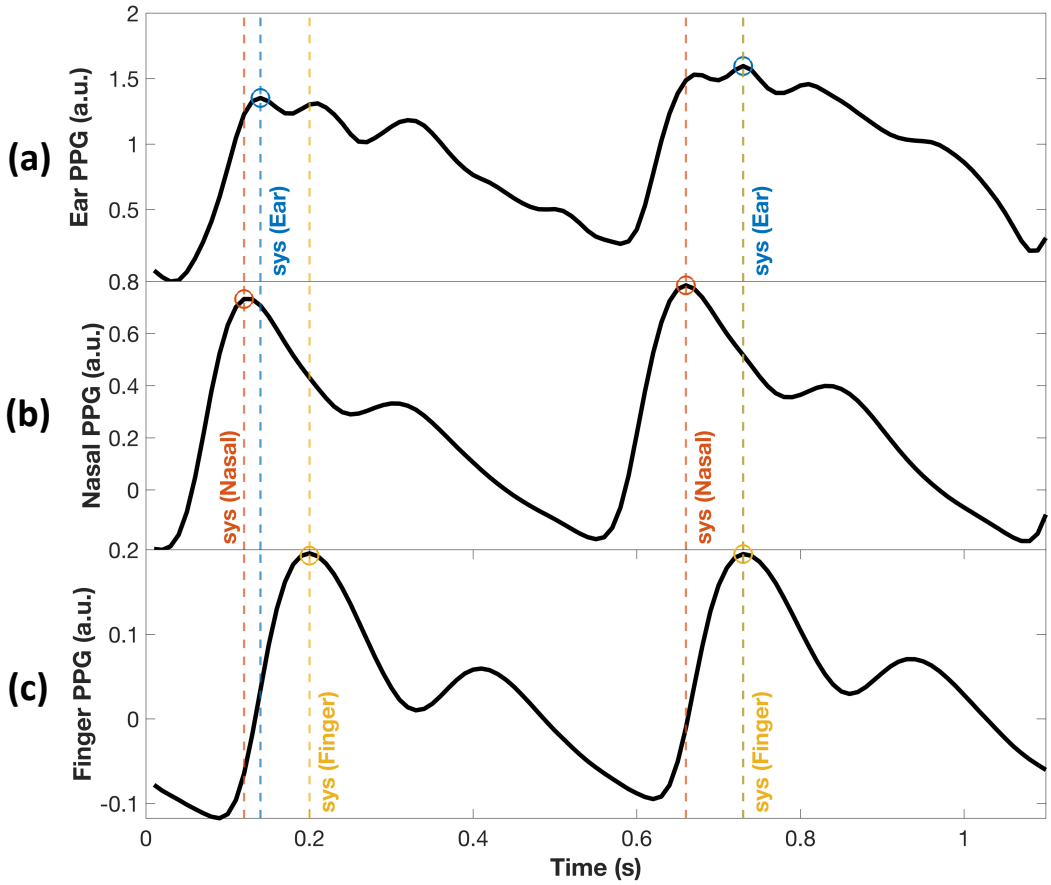

Figure 2: PPG signals with two cardiac cycles recorded from different body locations of a subject. The **sys** marked by the dashed lines are the **sys**'s detected from the ear PPG shown in (a). In the ear PPG, each cycle shows two local maxima around the locations where **sys** should exist. Notice that the first **sys** is detected at the first local maxima while the second **sys** is detected at the second local maxima. On the other hand, there is only one local maximum in the nasal PPG and finger PPG shown in (b) and (c) in this example. By visual inspection, clearly the location of **sys** for PPGs recorded from different body locations do not align. a.u. means arbitrary unit.

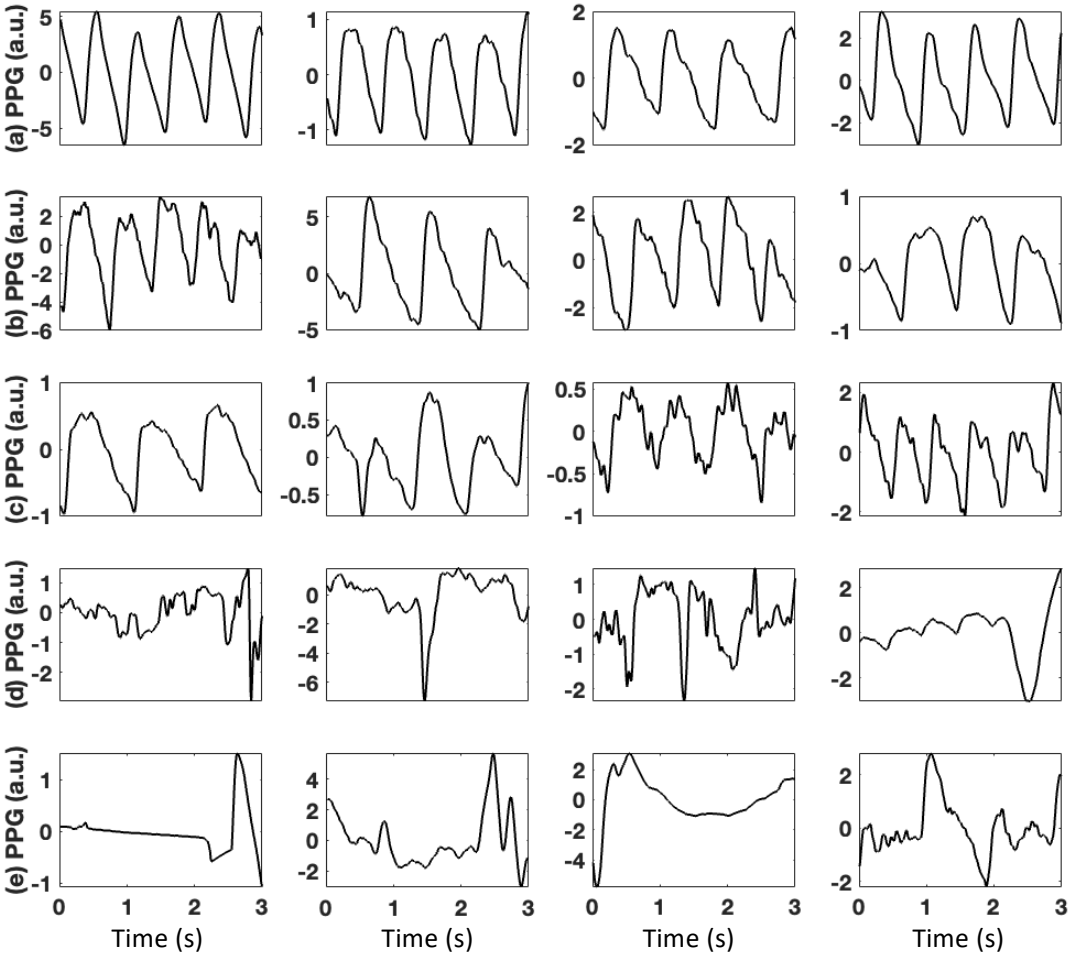

Figure 3: Ear PPG signals with an SQI of **(a)** 0.99, **(b)** 0.95, **(c)** 0.9, (d) 0.5, (e) 0.1.

a.u. means arbitrary unit.

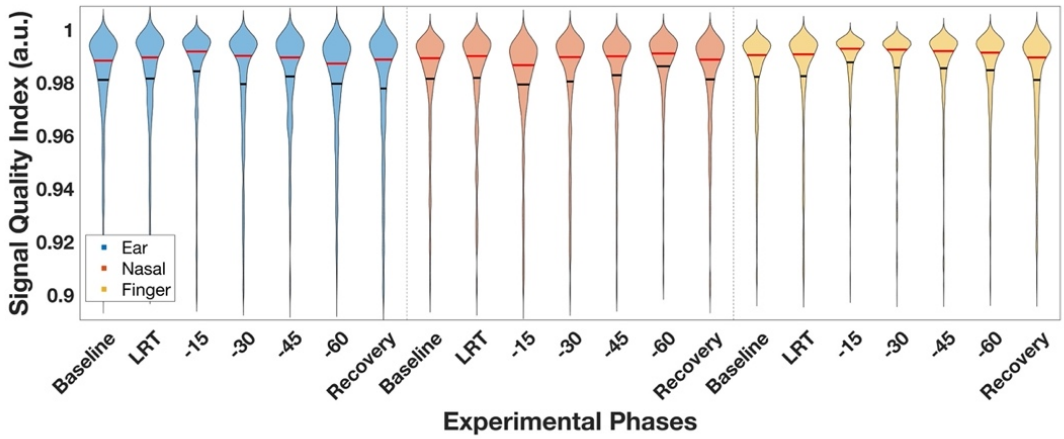

Figure 4: Progression of the distribution of signal quality index (SQI) over various experimental stages for different sensors. The solid red lines mark medians, while solid black lines mark means.

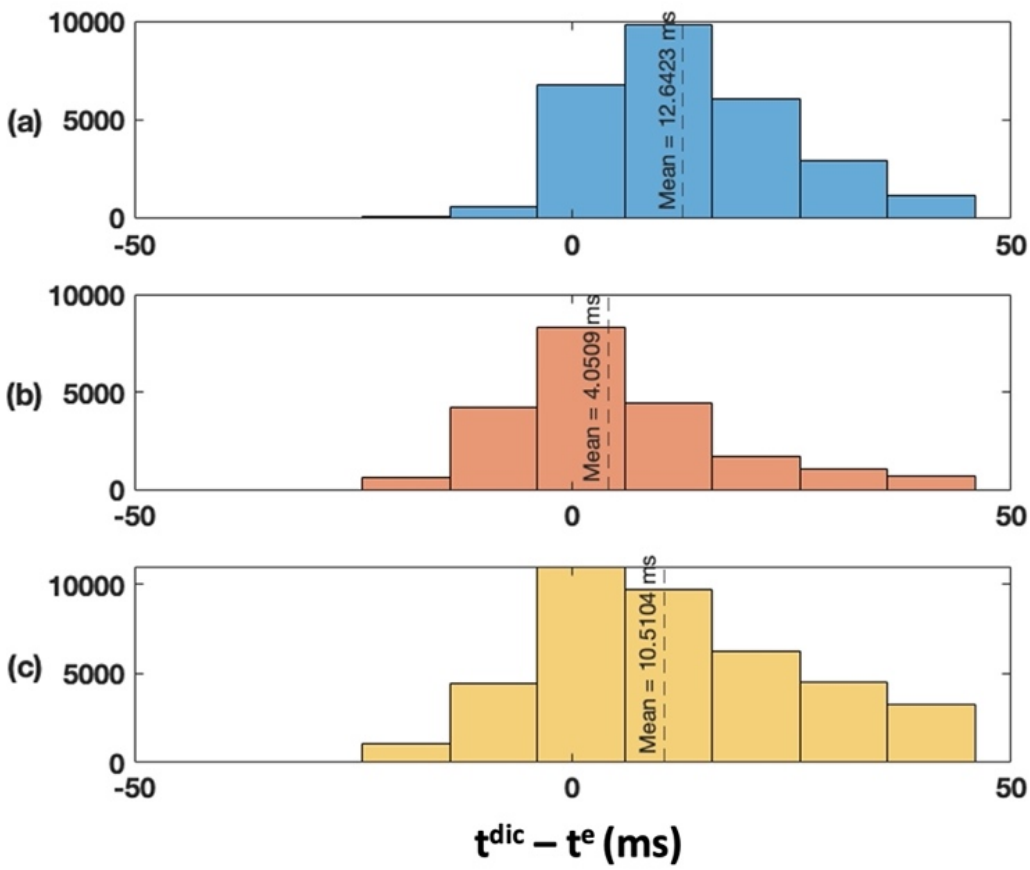

Figure 5: Histograms for the time difference between **dic** (t^{dic}) and the e point (t^{e}) for **(a)** ear PPG, **(b)** finger PPG, and **(c)** nasal PPG.

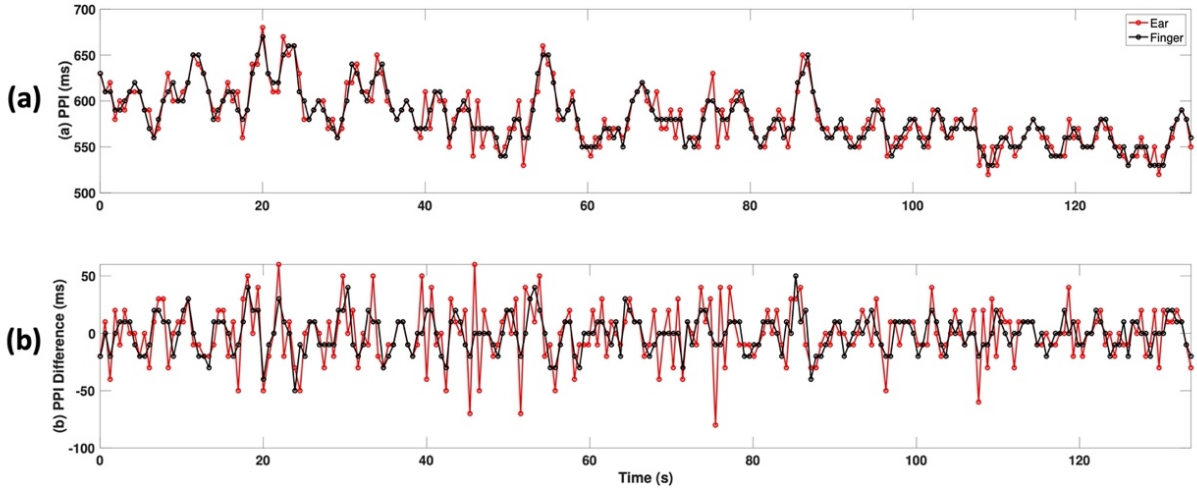

Figure 6: An illustration of pulse-to-pulse interval (PPI) shown in (a) and its derivative (dPPG) shown in (b). The red (black respectively) curves are PPI and dPPI derived from the ear (finger respectively) PPG.

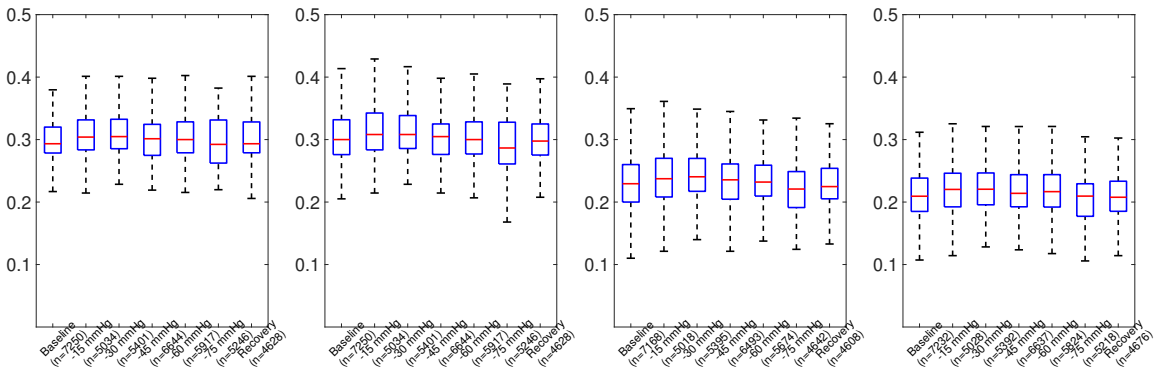

Figure 7: The boxplot of normalized PTT across different locations and LBNP stages. From left to right: Boxplots of normalized PTT across different LBNP stages, measured using Nellcor finger PPG, Xhale finger PPG, Xhale ear PPG and Xhale nose PPG, and Nellcor EKG. The normalized PTT, calculated using Nellcor finger PPG, Xhale finger PPG, Xhale ear PPG, and Xhale nose PPG, is 0.30±0.02, 0.30±0.03, 0.23±0.03, and 0.21±0.03 (no unit), respectively.

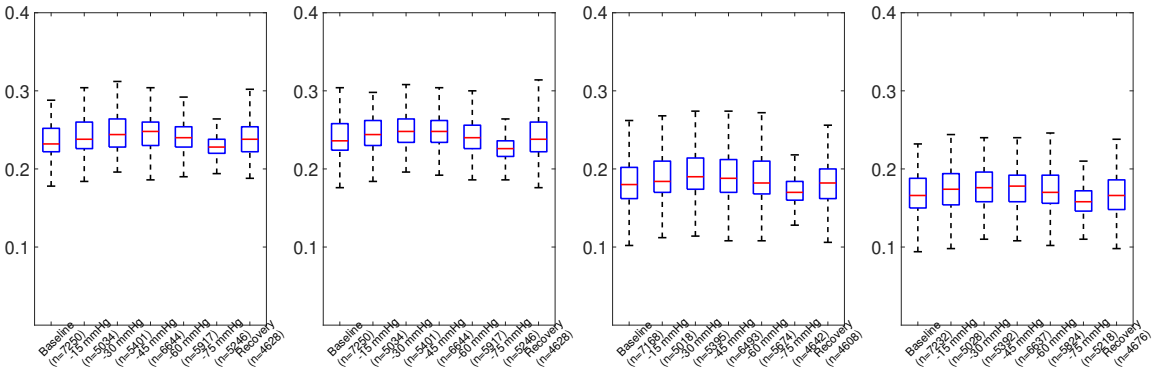

Figure 8: The boxplot of non-normalized PTT across different locations and LBNP stages. From left to right: Boxplots of non-normalized PTT across different LBNP stages, measured using Nellcor finger PPG, Xhale finger PPG, Xhale ear PPG and Xhale nose PPG, and Nellcor EKG. The non-normalized PTT, calculated using Nellcor finger PPG, Xhale finger PPG, Xhale ear PPG, and Xhale nose PPG, is 0.24±0.01, 0.24±0.02, 0.18±0.02, and 0.17±0.02 (sec), respectively.